Published in final edited form as:
*Gastrointest Endosc*. 2012 July ; 76(1): 32–40. doi:10.1016/j.gie.2012.02.003.

# Characterization of buried glands before and after radiofrequency ablation by using 3-dimensional optical coherence tomography (with videos)

**Chao Zhou, PhD**[1], **Tsung-Han Tsai, MS**[1], **Hsiang-Chieh Lee, MS**[1], **Tejas Kirtane, MD**[2], **Marisa Figueiredo, PA**[2], **Yuankai K. Tao, PhD**[1], **Osman O. Ahsen, BS**[1], **Desmond C. Adler, PhD**[3], **Joseph M. Schmitt, PhD**[3], **Qin Huang, MD**[2], **James G. Fujimoto, PhD**[1], and **Hiroshi Mashimo, MD, PhD**[2]
Cambridge, Boston, Westford, Massachusetts, USA

## Abstract

**Background—**Radiofrequency ablation (RFA) is an endoscopic technique used to eradicate Barrett's esophagus (BE). However, such ablation can commonly lead to neosquamous epithelium overlying residual BE glands not visible by conventional endoscopy and may evade detection on random biopsy samples.

**Objective—**To demonstrate the capability of endoscopic 3-dimensional optical coherence tomography (3D-OCT) for the identification and characterization of buried glands before and after RFA therapy.

**Design—**Cross-sectional study.

**Setting—**Single teaching hospital.

**Patients—**Twenty-six male and 1 female white patients with BE undergoing RFA treatment.

**Interventions—**3D-OCT was performed at the gastroesophageal junction in 18 patients before attaining complete eradication of intestinal metaplasia (pre–CE-IM group) and in 16 patients after CE-IM (post–CE-IM group).

**Main Outcome Measurements—**Prevalence, size, and location of buried glands relative to the squamocolumnar junction.

**Results—**3D-OCT provided an approximately 30 to 60 times larger field of view compared with jumbo and standard biopsy and sufficient imaging depth for detecting buried glands. Based on 3D-OCT results, buried glands were found in 72% of patients (13/18) in the pre–CE-IM group and 63% of patients (10/16) in the post–CE-IM group. The number (mean [standard deviation]) of buried glands per patient in the post–CE-IM group (7.1 [9.3]) was significantly lower compared



If you would like to chat with an author of this article, you may contact Dr Mashimo at hmashimo@hms.harvard.edu..
[1]Department of Electrical Engineering and Computer Science, Boston, MA, USA
[2]Research Laboratory of Electronics, Massachusetts Institute of Technology, Cambridge, Massachusetts, VA Boston Healthcare System , Boston, MA, USA
[3]Harvard Medical School, Boston, Massachusetts, LightLab Imaging , St Jude Medical, Inc, Westford, Massachusetts, USA.

DISCLOSURE: The following author disclosed financial relationships relevant to this publication: Dr. Fujimoto: LightLab Imaging Inc–St. Jude Medical, royalties from intellectual property owned by MIT and licensed to LightLab Imaging Inc; Carl Zeiss Meditec–St. Jude Medical, royalties from intellectual property owned by MIT and licensed to Carl Zeiss Meditec; scientific advisor to and stock options in Optovue, Inc. The other authors disclosed no financial relationships relevant to this publication.

Reprint requests: Hiroshi Mashimo, MD, PhD, Gastroenterology Section, VA Boston Healthcare System, Harvard School of Medicine, Boston, MA 02130.

with the pre–CE-IM group (34.4 [44.6]; $P = .02$). The buried gland size ($P = .69$) and distribution ($P = .54$) were not significantly different before and after CE-IM.

**Limitations—**A single-center, cross-sectional study comparing patients at different time points in treatment. Lack of 1-to-1 coregistered histology for all OCT data sets obtained in vivo.

**Conclusion—**Buried glands were frequently detected with 3D-OCT near the gastroesophageal junction before and after radiofrequency ablation.

Barrett's esophagus (BE) is a common condition associated with GERD,[1,2] in which the normal squamous epithelium of the esophagus is replaced by metaplastic columnar epithelium. In the United States, approximately 5.6% of the population is affected by this disease.[3] Patients with BE have an increased risk of the development of esophageal adenocarcinoma,[4] which is a fatal disease with a 5-year survival rate of less than 20%.[5] In the past 30 years, the incidence of esophageal adenocarcinoma in white men has increased 300% to 500%.[6,7]

Endoscopic surveillance biopsies are routinely performed to identify BE, which may be treated by using endoscopic ablative therapies,[8] such as argon plasma coagulation,[9] photodynamic therapy,[10] and radiofrequency ablation (RFA).[11-15] RFA uses an electrode array to deliver radiofrequency energy to the tissue surface. In a multicenter, sham-controlled trial, complete eradication of dysplasia was reported in 90.5% of patients with low-grade dysplasia (LGD) and in 81% of patients with high-grade dysplasia (HGD) 1 year after the initial RFA treatment.[14] After 3 years, complete eradication of dysplasia and complete eradication of intestinal metaplasia (CE-IM) was achieved in 98% and 91% of patients, respectively,[16] leading to increasing sentiment against further surveillance of HGD and toward ablative therapy. In another multicenter prospective trial, CE-IM was achieved at 2.5 years in 98.4% of patients with nondysplastic BE treated with RFA.[17] At 5-year follow-up, CE-IM was demonstrated in 92% of the patients.[15]

After RFA, new squamous epithelium generally replaces previous BE epithelium. However, residual BE glands can become "buried" by the neosquamous epithelium. These buried glands are not visible by conventional endoscopy, even when supplemented by chromogen or narrow-band imaging. The malignant potential of these buried glands is unknown,[18-20] but buried BE glands were found in 25.2% of patients before and in 5.1% of patients after successful RFA treatment when followed by 4-quadrant biopsies every 1 cm.[14] Although rigorous biopsies were performed over neosquamous epithelium after RFA treatment in study protocols,[14,15,21] these buried glands are likely underappreciated with the current surveillance protocol because areas of neosquamous epithelium do not routinely undergo biopsy in clinical practice. Furthermore, the sampling area and depth[15,21,22] of biopsy are limited, even with large-capacity forceps.

Optical coherence tomography (OCT)[23] is an emerging biomedical imaging technology that detects light backscattered from tissues to construct cross-sectional and 3-dimensional (3D) images of tissue microstructures with micron-scale resolution. Over the past decade, several groups have developed endoscopic OCT technologies for in vivo evaluation of disease and endoscopic therapies in the human GI tract.[24-31] OCT imaging depth is 1 to 2 mm in the human esophagus, enabling evaluation of tissue morphology underneath the squamous epithelium. The advent of high-speed endoscopic OCT systems,[28,30,32,33] enables 3D and comprehensive imaging. Because the location of buried glands is unpredictable, this imaging technology that uniquely enables depth-resolved imaging of a broad area with near-microscopic resolution holds great potential for identifying and characterizing buried glands before and after ablative therapies. We recently reported a case in which buried glands were

identified after RFA treatment.[31] In the current study, we further quantify our findings of buried glands by using 3D-OCT in a cohort of 27 patients undergoing RFA treatment.

## METHODS

### Endoscopic 3D-OCT system

Studies were performed by using an endoscopic 3D-OCT system developed in collaboration with LightLab Imaging–St. Jude Medical Inc (Westford, Mass) and described in previous publications.[30-32] The system used swept-source OCT with a Fourier-domain mode-locking laser[34] operating at a 1.3-$\mu$m center wavelength. The laser sweep rate was 60 kHz, and the sweep bandwidth supports a 5-$\mu$m axial resolution in tissue. The flexible OCT imaging probe, with an outer diameter of 2.5 mm, can be introduced through the biopsy channel of a standard endoscope. The probe focused an output beam of approximately 13 mW to an approximately 15-$\mu$m spot on the tissue, and the system had more than 100-dB sensitivity. The OCT beam was radially scanned at 60 Hz and pulled back at 1 mm/s, resulting in a 16-$\mu$m spacing between consecutive B-scan images. Each 3D-OCT data set, covering a region 8 mm (circumference) × 20 mm (length) × 2 mm (depth) was acquired in 20 seconds. Cross-sectional OCT images were displayed in real-time during the procedures, and a 3D-OCT data set was available for review immediately after the data were acquired. Quantification and characterization of the buried glands were performed during post-processing as described in the following.

### Patient enrollment and imaging procedures

The study was performed at the Boston Veterans Affair Healthcare System with protocol approvals from Boston Veterans Affair Healthcare System, Harvard Medical School, and Massachusetts Institute of Technology. Patients were diagnosed by using a standard white-light endoscope, and the length of visible BE was recorded based on the Prague C&M criteria.[35] Patients with raised lesions were excluded from the study. Twenty-seven patients, including 26 white male and 1 white female patient, undergoing RFA treatment were recruited (Table 1). Among them, 12 patients initially presented with long-segment BE and 15 patients with BE less than 2 cm. However, 3D-OCT imaging and our data analysis were limited to short-segment BE (≤2 cm) to ensure consistent OCT imaging probe placement at the gastroesophageal junction (GEJ). These included patients initially with long-segment BE that was later reduced to less than 2 cm by circumferential RFA treatment by using the BÂRRX HALO 360 catheter (BÂRRX Medical, Sunnyvale, Calif).

During each endoscopic procedure, the lower one third of the patient's esophagus was first surveyed with a high-definition white-light endoscope (Olympus GIF-Q180; Olympus America, Center Valley, Pa) by an experienced endoscopist. Multiple 3D-OCT data sets were acquired over different quadrants at the GEJ. After 3D-OCT imaging, BE regions identified endoscopically were ablated by using the BÂRRX HALO 90 catheter (BÂRRX Medical) with 300 W and 12 J/cm$^2$. The radiofrequency energy was delivered in 2 applications, with burned tissues rigorously scraped off between applications per standard protocol.[14] The patients underwent a follow-up endoscopy 6 to 8 weeks after RFA treatment. If no visible BE was identified endoscopically, random 4-quadrant biopsy samples were taken around the GEJ. The determination of CE-IM was based on endoscopic (no visible BE under white-light endoscopy and narrow-band imaging) as well as pathological findings (no intestinal metaplasia [IM] on pinch biopsy histology from the GEJ). The patient received additional RFA treatment if there was endoscopically visible BE or if IM was found based on histology. If CE-IM was achieved based on endoscopy and biopsy findings, the patient was followed 1 year later with standard endoscopy.

### Data analysis

Each 3D-OCT data set obtained at the GEJ was digitally unwrapped and flattened during after processing. A data set was excluded from subsequent analysis if the squamocolumnar junction (SCJ) was invisible or if severe image artifacts caused by nonuniform probe motion, air bubbles, or poor tissue contact were observed.

To characterize buried glands, 3D-OCT data sets were analyzed with Amira software (Visage Imaging, Inc, San Diego, Calif). Consistent with previous findings,[31,36] buried glands were identified from cross-sectional OCT images as poorly organized, sparsely distributed hyposcattering structures below the squamous epithelium within the lamina propria/muscularis mucosa with irregular size and shape. In contrast, blood vessels were identified as tubelike hyposcattering structures interconnected and branched in 3 dimensions. Esophageal glands were identified as deep and well-organized lobular structures below the lamina propria/muscularis mucosa. Buried glands and SCJ were labeled in each data set by using the segmentation tool provided in Amira software. The segmentation data were then loaded in MATLAB (MathWorks, Inc, Natick, Mass) to extract the number, size (the largest span of the buried glands in 3 dimensions), and the distance of the buried glands from the SCJ. When multiple 3D-OCT data sets were available for a patient at a single visit, the data set that showed the most buried glands was used for subsequent analysis. Average results from a group are presented as mean (standard deviation). The Student *t* test was used to statistically compare the number, size, and the distance of the buried glands from the SCJ between the pre–CE-IM and post–CE-IM groups. A $P$ value <.05 was used to determine statistical significance.

## RESULTS

Table 1 summarizes the patient demographic information. 3D-OCT was performed in 18 patients before CE-IM was achieved (pre–CE-IM group). Among these 18 patients, 7 were RFA-naive patients (no previous RFA treatment) and 11 had 1 or more RFA treatments before the first 3D-OCT (1.7 [1.2]). In the post–CE-IM group, 3D-OCT was performed in 16 patients who achieved CE-IM after a total of 2.6 (1.6) RFA procedures, including the original treatments to reduce the BE length to 2 cm or less. Note that 7 patients were included in both the pre– and post–CE-IM groups. The patient age in the 2 groups was comparable (65.3 [12.9] for pre–CE-IM group and 69.1 [11.8] for post–CE-IM group, $P = .37$). Before the initial RFA treatment in the pre–CE-IM group, 8 patients had BE without dysplasia, 6 had LGD, and 6 had HGD. Before initial RFA treatment in the post–CE-IM group, 7 patients had BE without dysplasia, 6 had LGD, and 3 had HGD. The BE lengths at initial diagnosis were 4.0 (4.0) cm and 4.0 (4.4) cm for the pre–CE-IM and post–CE-IM groups, respectively. The BE length at OCT imaging time point was 1.5 (0.6) cm for the pre–CE-IM group. On average, 2.1 (0.8) and 2.3 (0.9) 3D-OCT scans were performed during each procedure for the 2 groups, respectively. None of these differences between the 2 groups were statistically significant.

Figure 1 shows examples of cross-sectional OCT images and corresponding histology. Figure 1A,B was acquired in vivo at the position of the GEJ. Buried glands were identified with 3D-OCT at the GEJ of a patient during the imaging procedure. Landmarks of the OCT imaging site were visually identified under EGD. The OCT probe was then retracted from the working channel of the GIF-Q180 endoscope, and biopsy forceps were inserted through the same channel. Pinch biopsy samples were taken from the OCT imaging site with direct visualization on EGD. The histological micrograph shown in Figure 1C confirmed the presence of buried glands with IM underneath neosquamous epithelium. Figure 1D,E was obtained from an ex vivo EMR specimen to enable more accurate correspondence of OCT images with histology. From cross-sectional OCT images, squamous epithelium is

characterized by a low-scattering, homogeneous layer at the mucosal surface. Buried glands were identified as sparsely distributed hyposcattering structures underneath the squamous epithelium with various sizes and shapes. The histological micrograph of the EMR specimen (Fig. 1F) also confirmed the presence of buried glands with IM.

Figure 2 shows OCT images from a patient in the pre–CE-IM group. Figure 2A is an en face OCT image that is the projection of the logarithm-compressed 3D-OCT image over the full axial depth imaging range. Here, columnar epithelium corresponds to BE, and squamous epithelium as well as the SCJ can be clearly identified. The locations of the buried glands are indicated. Cross-sectional OCT images corresponding to those in Figure 2A are shown in Figure 2B,C. Buried glands are clustered under the squamous epithelium. The lamina propria/muscularis mucosa layer exhibited strong backscattering OCT signals because of the rich collagen content. The lamina propria/muscularis mucosal layer was clearly observed in 3D-OCT data sets obtained from all 27 patients, suggesting that OCT has sufficient imaging depth for evaluation of buried glands. Figure 2D,E are 3× zoomed views of the regions with buried glands shown in Figure 2B,C, respectively. A double-band feature, also described by other groups,[36] can be observed from some glands. To further demonstrate these buried glands in 3 dimensions, a video of cross-sectional OCT images scanning through the SCJ is provided in Video 1 (available online at www.giejournal.org). The 3D-OCT data set proved to be very useful for differentiating buried glands from blood vessels, which are interconnected and branched in 3 dimensions, and from esophageal glands, which are deep, lobular, and well organized with sharp borders.

Figure 3 shows another example from a patient in the post–CE-IM group. The columnar epithelium, (corresponds to the gastric mucosa), squamous epithelium, and the SCJ are seen from the en face projection OCT image (Fig. 3A). Buried glands appear to be fewer and scattered near the squamous epithelium. Cross-sectional OCT images in Figure 3B-E show these buried glands in more detail. Video 2 (available online at www.giejournal.org) shows cross-sectional OCT images scanning through the buried glands.

In the entire patient cohort, buried glands were identified in 72% patients (13/18) in the pre–CE-IM group and 63% patients (10/16) in the post–CE-IM group. Furthermore, as shown in Figure 4, the number of buried glands per patient observed in the post–CE-IM group (7.1 [9.3], median = 5) is significantly lower compared with the number of buried glands per patient observed in the pre–CE-IM group (34.4 [44.6], median = 26.5; $P = .02$).

Overall, 620 and 114 buried glands were marked in 3D-OCT data sets from patients in the pre–CE-IM and post–CE-IM groups, respectively. For comparison, Figure 5 shows histograms of the gland sizes (Fig. 5A) and the distance from the SCJ (Fig. 5B). Both groups demonstrate a single peak of approximately 180 $\mu$m in the gland size distribution. On average, the size of the buried glands is 214 (126) $\mu$m in the pre–CE-IM group, and 219 (111) $\mu$m in the post–CE-IM group, respectively. The gland sizes before and after CE-IM are not significantly different ($P = .69$). Furthermore, as shown in Figure 5B, the distribution of the buried glands relative to the SCJ is also similar in both groups. Sixty-seven percent (415/620) and 69% (79/114) of the glands were observed within 5 mm of the SCJ in the pre–CE-IM group and post–CE-IM group, respectively. The average distance of these glands from the SCJ is 3.6 (2.7) mm in the pre–CE-IM group and 3.8 (3.9) mm in the post–CE-IM group and was not statistically significant between the 2 groups ($P = .54$).

## DISCUSSION

In this study, in vivo characterization of buried glands in BE patients treated with RFA was performed by using high-speed, endoscopic 3D-OCT. A higher prevalence of buried glands

in both the pre–CE-IM (72%) and the post–CE-IM groups (63%) was observed compared with previous reports by performing 4-quadrant biopsies every 1 cm (up to 25% pre– and none to 5% post–CE-IM).[14,15,21] Higher prevalence is expected in our study because the area of the distal esophagus imaged with 3D-OCT is considerably larger and more comprehensive than that with pinch biopsies. Each 3D-OCT data set provides approximately 160 $mm^2$ (8-mm circumference × 20-mm pullback) coverage of the esophagus if the tissue is fully wrapped around the probe. This is approximately 30 to 60 times larger than the area sampled by jumbo biopsy forceps (~6 $mm^2$) and standard biopsy forceps (~2.5 $mm^2$). However, because the human esophagus is approximately 1.5 to 2 cm in diameter, each scan using the current OCT probe design only covers 1/6 to 1/8 of the esophageal circumference. Therefore, it is important to image different quadrants of the esophagus to maximize the coverage area and decrease sampling errors. The lamina propria/muscularis mucosa of the esophagus was visible in all OCT data sets collected in this study, suggesting the penetration depth of OCT was sufficient to evaluate the buried glands. In contrast, only 40% to 80% of biopsies reached the lamina propria or deeper, as reported in recent studies.[21,37] In addition, Cobb et al[36] recently found buried glands by using OCT in 10 of 14 ex vivo esophagectomy specimens by focused sampling in areas near the SCJ. The high prevalence of buried glands reported in their study is consistent with our findings. The high probability of finding buried glands near the SCJ was also confirmed with our buried gland distribution results, in which 67% and 69% of these glands were found within 5 mm from the SCJ in the pre–CE-IM and post–CE-IM groups, respectively.

Although we have shown that the number of buried glands per patient is significantly lower after CE-IM is achieved, buried glands still exist in a high percentage of patients post–CE-IM. These glands may disappear over time without treatment, grow as recurrent BE, or even become malignant. Further investigation is needed to understand the longitudinal progression of the buried glands in the same patient over time. One hypothesis is that patients with a large number of buried glands are at higher risk of recurrent BE or malignant progression. If this proves to be true, the information on buried glands that OCT provides may be used to stratify the patient risk, as suggested by a recent editorial[38] and could even help direct areas for re-ablation. Repeated treatment or close surveillance may be used for high-risk patients, whereas longer surveillance may be used for low-risk patients to improve the cost-effectiveness in the current paradigm for BE management. Furthermore, OCT is a minimally invasive method to evaluate buried glands or other subsurface features and may be used to evaluate the efficacy of other endoscopic therapies, such as cryoablation[39,40] and photodynamic therapies.[10]

There are several limitations to the current study. First, the study was performed without coregistered histology of the buried glands observed in the OCT data sets. This is because of the procedural difficulties of performing biopsy simultaneously with OCT imaging and using OCT to guide the biopsy, as well as the small size and area coverage of biopsy forceps. To address this limitation, OCT images and corresponding histology are presented from 1 biopsy specimen in vivo and 1 ex vivo EMR specimen obtained at the GEJ (Fig. 1). In both cases, histology showed buried glands with IM. With the current image resolution, OCT is not capable of differentiating glandular mucosa with or without IM. Compared with gastric glandular mucosa or superficial esophageal glands, however, glands with IM are often dilated, irregular, and sparsely distributed in the superficial part of the lamina propria. The buried glands observed on OCT are irregular and sparsely distributed and likely correspond to these dilated glands. In addition, we observed the same imaging features for buried glands compared with a recent ex vivo OCT imaging study that used esophagectomy specimens.[36] Furthermore, considering that the areas underneath the neosquamous epithelium were columnar epithelium before the RFA treatment, glandular structures underneath the neosquamous epithelium observed after RFA treatments are likely buried BE

glands rather than normal buried glandular mucosa. In the future, a dual-channel endoscope may be used to enable image-guided pinch biopsy by using OCT. Improved matching of OCT images obtained in vivo and histology should then be obtained. Further improvement in image resolution and the development of more specific imaging technology such as polarization-sensitive OCT may also help improve the accuracy of the detection of buried glands.

A second limitation is that this was a cross-sectional study comparing patients at different time points in treatment. Because of the variations in the extent of BE at initial presentation as well as variations in the number of RFA treatments needed to achieve CE-IM, the study recruited both RFA-naive and previously treated patients focusing on those with short-segment BE. This was done because this represents a treatment point at which the OCT imaging probe could be consistently placed at the GEJ. Variations in disease severity and response across the patient population contribute to the variations in the data. 3D-OCT imaging is performed before and after a varying number of RFA treatments, so that the data are not necessarily representative of either a single RFA treatment or the entire course of RFA treatments starting from treatment-naive patients. However, buried glands were found in 6 of the 7 RFA-naive patients (86%) in the pre–CE-IM group. In addition, the number of buried glands observed per patient (36.1 [35.1], median = 23) in these RFA-naive patients was not significantly different from the statistics including all the patients in the pre–CE-IM group (34.4 [44.6], median = 26.5; $P = .93$).

Finally, this was a single-center study with a relatively small cohort of patients. A more rigorous, multicenter, longitudinal clinical study is needed to further establish the utility of endoscopic 3D-OCT for the management of BE in clinical practice.

## CONCLUSION

In summary, this study demonstrates that 3D-OCT provides a 30 to 60 times larger field of view compared with jumbo and standard forceps biopsy and sufficient imaging depth to the lamina propria/muscularis mucosa to facilitate the detection of buried glands pre– and post–CE-IM. A high prevalence of buried glands in 72% patients in the pre–CE-IM group and in 63% patients in the post–CE-IM group was observed. This high prevalence is consistent with biopsy results from previous studies when accounting for the differences in sampling area between OCT imaging and excisional biopsy. The number of buried glands per patient decreased significantly after CE-IM is achieved ($P = .02$). However, the size and distribution of the buried glands relative to the SCJ in patients with short-segment BE did not change significantly post–CE-IM. Further investigation is needed to understand the longitudinal progression and clinical implications of buried glands.

## Supplementary Material

Refer to Web version on PubMed Central for supplementary material.

## Acknowledgments

The authors acknowledge the facility support from the VA Boston Healthcare System. NIH grants R01-CA75289-15 (J.G.F., H.M.), R44CA101067-06, R01-HL095717-03, R01-NS057476-05, and K99-EB010071-01A1, Air Force Office of Scientific Research contract FA9550-10-1-0063 (J.G.F.), Medical Free Electron Laser Program contract FA9550-10-1-0551 (J.G.F.), and the MIT/CIMIT Medical Engineering Fellowship.

## Abbreviations

| | |
|---|---|
| **3D** | 3-dimensional |
| **BE** | Barrett's esophagus |
| **CE-IM** | complete eradication of intestinal metaplasia |
| **GEJ** | gastroesophageal junction |
| **HGD** | high-grade dysplasia |
| **IM** | intestinal metaplasia |
| **LGD** | low-grade dysplasia |
| **OCT** | optical coherence tomography |
| **RFA** | radiofrequency ablation |
| **SCJ** | squamocolumnar junction. |

## REFERENCES


1. Allison PR, Johnstone AS. The oesophagus lined with gastric mucous membrane. Thorax. 1953; 8:87–101. [PubMed: 13077502]
2. Reid BJ, Li XH, Galipeau PC, et al. Barrett's oesophagus and oesophageal adenocarcinoma: time for a new synthesis. Nat Rev Cancer. 2010; 10:87–101. [PubMed: 20094044]
3. Hayeck TJ, Kong CY, Spechler SJ, et al. The prevalence of Barrett's esophagus in the US: estimates from a simulation model confirmed by SEER data. Dis Esophagus. 2010; 23:451–7. [PubMed: 20353441]
4. Naef AP, Savary M, Ozzello L. Columnar-lined lower esophagus: acquired lesion with malignant predisposition. Report on 140 cases of Barrett's esophagus with 12 adenocarcinomas. J Thorac Cardiovasc Surg. 1975; 70:826–35. [PubMed: 1186274]
5. Esophageal Cancer. American Cancer Society; Available at: www.cancer.org
6. Devesa SS, Blot WJ, Fraumeni JF Jr. Changing patterns in the incidence of esophageal and gastric carcinoma in the United States. Cancer. 1998; 83:2049–53. [PubMed: 9827707]
7. Shaheen N, Ransohoff DF. Gastroesophageal reflux, Barrett esophagus, and esophageal cancer: clinical applications. JAMA. 2002; 287:1982–6. [PubMed: 11960541]
8. Johnston MH. Technology insight: ablative techniques for Barrett's esophagus–current and emerging trends. Nature clinical practice. 2005; 2:323–30.
9. Van Laethem JL, Cremer M, Peny MO, et al. Eradication of Barrett's mucosa with argon plasma coagulation and acid suppression: immediate and mid term results. Gut. 1998; 43:747–51. [PubMed: 9824599]
10. Overholt BF, Lightdale CJ, Wang KK, et al. Photodynamic therapy with porfimer sodium for ablation of high-grade dysplasia in Barrett's esophagus: international, partially blinded, randomized phase III trial. Gastrointest Endosc. 2005; 62:488–98. [PubMed: 16185958]
11. Dunkin BJ, Martinez J, Bejarano PA, et al. Thin-layer ablation of human esophageal epithelium using a bipolar radiofrequency balloon device. Surg Endosc. 2006; 20:125–30. [PubMed: 16333533]
12. Sharma VK, Wang KK, Overholt BF, et al. Balloon-based, circumferential, endoscopic radiofrequency ablation of Barrett's esophagus: 1-year follow-up of 100 patients. Gastrointest Endosc. 2007; 65:185–95. [PubMed: 17258973]
13. Ganz RA, Overholt BF, Sharma VK, et al. Circumferential ablation of Barrett's esophagus that contains high-grade dysplasia: a U.S. Multicenter Registry. Gastrointest Endosc. 2008; 68:35–40. [PubMed: 18355819]
14. Shaheen NJ, Sharma P, Overholt BF, et al. Radiofrequency ablation in Barrett's esophagus with dysplasia. N Engl J Med. 2009; 360:2277–88. [PubMed: 19474425]

15. Fleischer DE, Overholt BF, Sharma VK, et al. Endoscopic radiofrequency ablation for Barrett's esophagus: 5-year outcomes from a prospective multicenter trial. Endoscopy. 2010; 42:781–9. [PubMed: 20857372]
16. Shaheen NJ, Overholt BF, Sampliner RE, et al. Durability of radiofrequency ablation in Barrett's esophagus with dysplasia. Gastroenterology. 2011; 141:460–8. [PubMed: 21679712]
17. Fleischer DE, Overholt BF, Sharma VK, et al. Endoscopic ablation of Barrett's esophagus: a multicenter study with 2.5-year follow-up. Gastrointest Endosc. 2008; 68:867–76. [PubMed: 18561930]
18. Yachimski P, Falk GW. Subsquamous intestinal metaplasia: implications for endoscopic management of Barrett's esophagus. Clin Gastroenterol Hepatol. 2012; 10:220–4. [PubMed: 22020059]
19. Chennat J, Ross AS, Konda VJ, et al. Advanced pathology under squamous epithelium on initial EMR specimens in patients with Barrett's esophagus and high-grade dysplasia or intramucosal carcinoma: implications for surveillance and endotherapy management. Gastrointest Endosc. 2009; 70:417–21. [PubMed: 19555948]
20. Gray NA, Odze RD, Spechler SJ. Buried metaplasia after endoscopic ablation of Barrett's esophagus: a systematic review. Am J Gastroenterol. 2011; 106:1899–908. quiz 1909. [PubMed: 21826111]
21. Pouw RE, Gondrie JJ, Rygiel AM, et al. Properties of the neosquamous epithelium after radiofrequency ablation of Barrett's esophagus containing neoplasia. Am J Gastroenterol. 2009; 104:1366–73. [PubMed: 19491850]
22. Shaheen NJ, Peery AF, Overholt BF, et al. Biopsy depth after radiofrequency ablation of dysplastic Barrett's esophagus. Gastrointest Endosc. 2010; 72:490–6. [PubMed: 20598302]
23. Huang D, Swanson EA, Lin CP, et al. Optical coherence tomography. Science. 1991; 254:1178–81. [PubMed: 1957169]
24. Rollins AM, Ung-Arunyawee R, Chak A, et al. Real-time in vivo imaging of human gastrointestinal ultrastructure by use of endoscopic optical coherence tomography with a novel efficient interferometer design. Opt Lett. 1999; 24:1358–60. [PubMed: 18079803]
25. Li XD, Boppart SA, Van Dam J, et al. Optical coherence tomography: advanced technology for the endoscopic imaging of Barrett's esophagus. Endoscopy. 2000; 32:921–30. [PubMed: 11147939]
26. Bouma BE, Tearney GJ, Compton CC, et al. High-resolution imaging of the human esophagus and stomach in vivo using optical coherence tomography. Gastrointest Endosc. 2000; 51:467–74. [PubMed: 10744824]
27. Chen Y, Aguirre AD, Hsiung PL, et al. Ultrahigh resolution optical coherence tomography of Barrett's esophagus: preliminary descriptive clinical study correlating images with histology. Endoscopy. 2007; 39:599–605. [PubMed: 17611914]
28. Suter MJ, Vakoc BJ, Yachimski PS, et al. Comprehensive microscopy of the esophagus in human patients with optical frequency domain imaging. Gastrointest Endosc. 2008; 68:745–53. [PubMed: 18926183]
29. Zhou C, Adler DC, Becker L, et al. Effective treatment of chronic radiation proctitis using radiofrequency ablation. Therap Adv Gastroenterol. 2009; 2:149–56.
30. Adler DC, Zhou C, Tsai TH, et al. Three-dimensional endomicroscopy of the human colon using optical coherence tomography. Opt Express. 2009; 17:784–96. [PubMed: 19158891]
31. Adler DC, Zhou C, Tsai TH, et al. Three-dimensional optical coherence tomography of Barrett's esophagus and buried glands beneath neosquamous epithelium following radiofrequency ablation. Endoscopy. 2009; 41:773–6. [PubMed: 19746317]
32. Adler DC, Chen Y, Huber R, et al. Three-dimensional endomicroscopy using optical coherence tomography. Nat Photonics. 2007; 1:709–16.
33. Vakoc BJ, Shishko M, Yun SH, et al. Comprehensive esophageal microscopy by using optical frequency-domain imaging (with video). Gastrointest Endosc. 2007; 65:898–905. [PubMed: 17383652]
34. Huber R, Wojtkowski M, Fujimoto JG. Fourier Domain Mode Locking (FDML): a new laser operating regime and applications for optical coherence tomography. Opt Express. 2006; 14:3225–37. [PubMed: 19516464]

35. Sharma P, Dent J, Armstrong D, et al. The development and validation of an endoscopic grading system for Barrett's esophagus: the Prague C & M criteria. Gastroenterology. 2006; 131:1392–9. [PubMed: 17101315]

36. Cobb MJ, Hwang JH, Upton MP, et al. Imaging of subsquamous Barrett's epithelium with ultrahigh-resolution optical coherence tomography: a histologic correlation study. Gastrointest Endosc. 2010; 71:223–30. [PubMed: 19846077]

37. Shaheen NJ, Peery AF, Overholt BF, et al. Biopsy depth after radiofrequency ablation of dysplastic Barrett's esophagus. Gastrointest Endosc. 2010; 72:490–6. [PubMed: 20598302]

38. Peery AF, Shaheen NJ. Optical coherence tomography in Barrett's esophagus: the road to clinical utility. Gastrointest Endosc. 2010; 71:231–4. [PubMed: 20152306]

39. Johnston MH, Eastone JA, Horwhat JD, et al. Cryoablation of Barrett's esophagus: a pilot study. Gastrointest Endosc. 2005; 62:842–8. [PubMed: 16301023]

40. Dumot JA, Vargo JJ 2nd, Falk GW, et al. An open-label, prospective trial of cryospray ablation for Barrett's esophagus high-grade dysplasia and early esophageal cancer in high-risk patients. Gastrointest Endosc. 2009; 70:635–44. [PubMed: 19559428]

**Take-home Message**

- The prevalence of buried glands in patients in whom complete eradication of intestinal metaplasia was achieved after radiofrequency ablation is higher than previously reported using standard 4-quadrant biopsies.
- 3-Dimensional optical coherence tomography may be used to evaluate treatment efficacy and guide endoscopic therapies in the future.

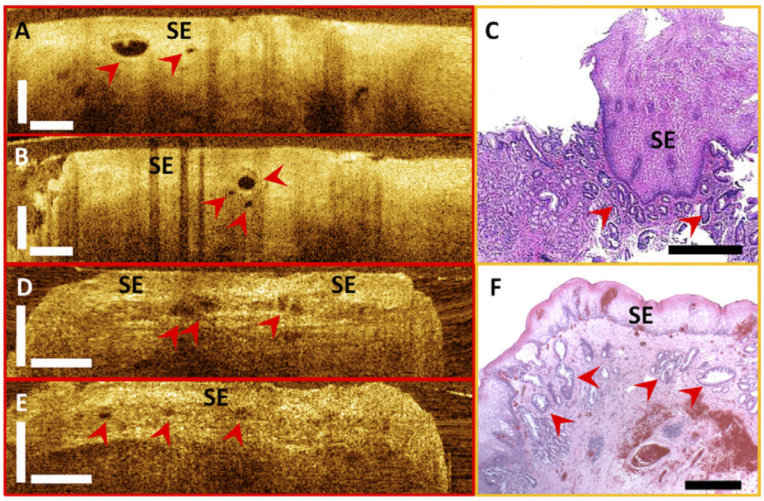


**Figure 1.**

Cross-sectional optical coherence tomography images and corresponding histology showing buried glands (*red arrowheads*) from 1 patient in vivo (**A**-**C**) and 1 ex vivo EMR specimen (**D**-**F**). **C**, **F,** Histological micrographs confirmed the presence of buried glands with intestinal metaplasia. SE, squamous epithelium. Scale bars, 500 $\mu$m.

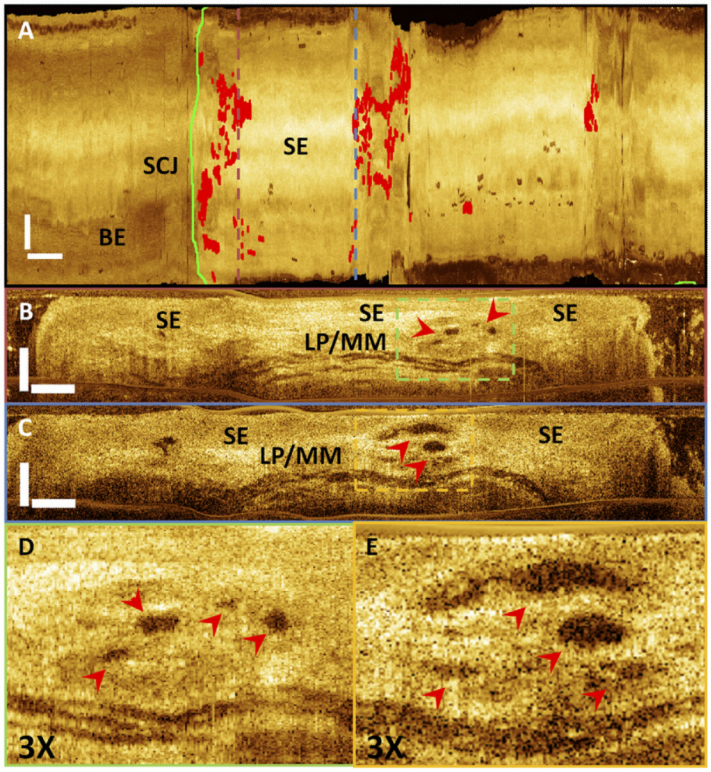


**Figure 2.**

Optical coherence tomography (OCT) images from a patient in the pre–CE-IM (complete eradication of intestinal metaplasia) group. **A,** En face projection over the full imaging depth of the 3-dimensional OCT data (log OCT signal). The squamocolumnar junction (SCJ) is indicated by the *green line*, with columnar epithelium on the left (corresponds to Barrett's esophagus [BE]) and squamous epithelium (SE) on the right. *Red dots* indicate buried glands. **B, C,** Cross-sectional OCT images corresponding to the *dashed brown and blue lines* in **A**. The *red arrowheads* indicate buried glands. **D** and **E,** Zoomed views (3×) of the regions of buried glands shown in **B** and **C**. LP/MM, lamina propria/muscularis mucosa. Scale bars: **A,** 1 mm; **B** and **C,** 500 $\mu$m. (Video 1 scans through the SCJ showing buried glands.)

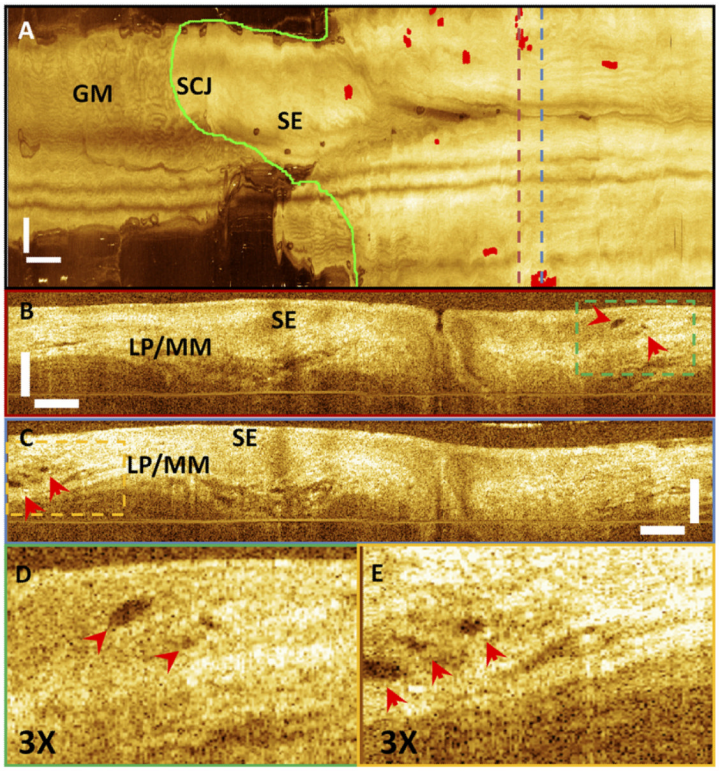


**Figure 3.**

Optical coherence tomography (OCT) images from a patient in the post–CE-IM (complete eradication of intestinal metaplasia) group. **A,** En face projection over the full depth range of the 3-dimensional OCT data (log OCT signal). The squamocolumnar junction (SCJ) is indicated by the *green line* with columnar epithelium on the left (corresponds to gastric mucosa [GM]) and squamous epithelium (SE) on the right. *Red dots* indicate buried glands. **B, C,** Cross-sectional OCT images corresponding to the *dashed brown and blue lines* in **A**. The *red arrowheads* indicate buried glands. **D** and **E,** Zoomed views (3×) of the region of buried glands shown in **B** and **C**. LP/MM, lamina propria/muscularis mucosa. Scale bars: **A,** 1 mm; **B** and **C,** 500 $\mu$m. (Video 2 scans through the buried glands post CE-IM.)

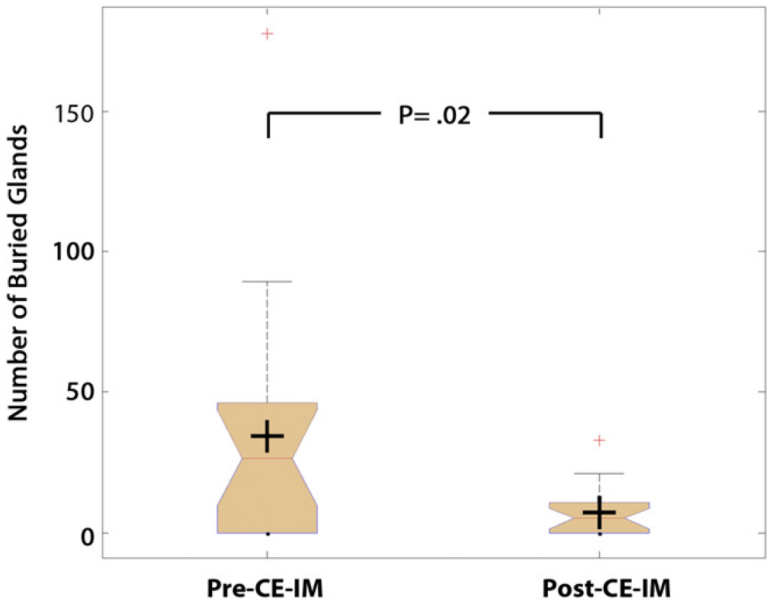


**Figure 4.**

Comparison of the number of buried glands observed per patient in the pre–CE-IM (complete eradication of intestinal metaplasia) and post–CE-IM groups. The number of buried glands per patient was significantly lower in the post–CE-IM group (7.1 [9.3], median = 5) compared with the pre–CE-IM group (34.4 [44.6], median = 26.5; $P = .02$).

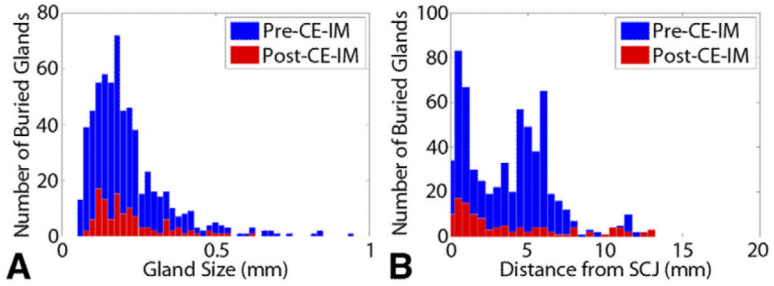


**Figure 5.**

Histograms of **(A)** the buried gland size and **(B)** distance from the squamocolumnar junction (SCJ) in the pre–CE-IM (complete eradication of intestinal metaplasia) and post–CE-IM groups. No significant difference was observed in either the gland size or gland distribution between the 2 groups.

**TABLE 1**

Patient demographic information |

| | Group | | |
|---|---|---|---|
| | **Pre–CE-IM** | **Post–CE-IM** | ***t* test** |
| Enrollment | n = 18, *(7 RFA naive, 11 with previous RFA | n = 16 * | – |
| Age, y | | | |
| Mean (SD) | 65.3(12.9) | 69.1 (11.8) | *P* = .37 |
| Range | 32-91 | 49-91 | |
| Sex, male/female | 17/1 | 16/0 | – |
| Race, white | 18 | 16 | – |
| Initial diagnosis | | | |
| BE without dysplasia | 8 | 7 | – |
| LGD | 4 | 6 | – |
| HGD | 6 | 3 | – |
| BE length at initial diagnosis, cm | | | |
| Mean (SD) | 4.0 (4.0) | 4.0 (4.4) | *P* = .98 |
| Range | 0.5-14 | 0.5-14 | |
| BE length at OCT imaging, cm | | | – |
| Mean (SD) | 1.5 (0.6) | – | |
| Range | 0.5-2 | | |
| No. of RFA before OCT imagingf | | | – |
| Mean (SD) | 1.7 (1.2)≠ | – | |
| Range | 1-5 | | |
| No. of RFA before CE-IMf | | | |
| Mean (SD) | – | 2.6(1.6) | – |
| Range | | 1-7 | |
| No. of 3D-OCT scans at GEJ | | | |
| Mean (SD) | 2.1 (0.8) | 2.3 (0.9) | *P* = .38 |
| Range | 1-3 | 1-4 | |

*CE-IM,* Complete eradication of intestinal metaplasia; *RFA,* radiofrequency ablation; SD, standard deviation; *BE,* Barrett's esophagus; *LGD,* low-grade dysplasia; *HGD,* high-grade dysplasia; OCT, optical coherence tomography; *3D-OCT,* 3-dimensional optical coherence tomography; *GEJ,* gastroesophageal junction.

*Seven patients were included in both the pre-CE-IM group and the post-CE-IM group.

†Include both HALO 360 and HALO 90 treatments.

‡Does not include the 7 RFA-naive patients.